Chinese Chemical Letters 33 (2022) 983–986

Contents lists available at ScienceDirect

Chinese Chemical Letters

journal homepage: www.elsevier.com/locate/cclet

Label-free photoelectrochemical sensor based on 2D/2D $ZnIn_2S_4$/g-C_3N_4 heterojunction for the efficient and sensitive detection of bisphenol A

Qiaowei Chen, Chen Yuan, Chunyang Zhai*

School of Materials Science and Chemical Engineering, Ningbo University, Ningbo 315211, China

ARTICLE INFO

Article history:
Received 30 April 2021
Revised 28 June 2021
Accepted 19 July 2021
Available online 27 July 2021

Keywords:
Bisphenol A
$ZnIn_2S_4$/g-C_3N_4
Heterojunction
Photoelectrochemical sensor

ABSTRACT

Photoelectrochemical (PEC) sensor is an emerging technology in analysis as the advantage of fast response, high sensitivity and uncomplicated operation. In this study, an effective label-free PEC sensor for bisphenol A (BPA) detecting is constructed, in which $ZnIn_2S_4$/g-C_3N_4 heterojunction is prepared *via* a simple hydrothermal method. The characterization outcomes display that the formation of p-n heterojunction helps for promoting the separation efficiency of photo-generated carrier. Under visible light irradiation, the $ZnIn_2S_4$/g-C_3N_4 modified electrode exhibits broader liner range from 0.05 mmol/L to 30 mmol/L and lower detection limit of 0.016 μmol/L (S/N=3) with remarkable stability and reproducibility of detection BPA under visible light irradiation. Furthermore, the constructed PEC sensor displays favorable potential for detection of BPA in practical applications.

Bisphenol A (BPA, 2,2-bis(4-hydroxyphenyl)propane), an important organic chemical raw material, is always found in much food and drink packaging products [1]. A small amount of BPA could release into food or drink water from food or drink containers due to its high temperature intolerance [2]. However, as an estrogen mimic, BPA may cause imbalance in the endocrine system, immune system and nervous system even at a lower dose of exposure [3]. So that, it is extremely urgent to establish rapid, reliable and simple analytical method to detect BPA in an aquatic environment.

Recently, photoelectrochemical (PEC) sensors, due to the unique separation process of input (light source) and output (electrical) signals, which is given many advantages of almost inappreciable background signals, cheap devices and rapidly high sensitivity, have developed into an effective analytical technology to detect BPA [4–6]. It is noteworthy that the reasoning design and synthesis of photoanode material is considered as a committed step in the process of PEC detecting BPA. Diverse types of photoactive materials, including carbon materials [7,8], noble metal nanoparticles [9,10] and semiconductor materials [11–13], have been used as photoanode in PEC sensor for determining BPA. Among them, semiconductor heterojunction has won great attention for its efficient photoelectron/hole pair migration, broadened light absorption range and excellent PEC performance, which shown charming potential in photocatalytic hydrogen generation [14–17], photocatalytic degradation of pollutants [18–22] and PEC detection [4,23,24]. For instance, Zhang *et al.* [13] successfully designed a novel hierarchical hollow ZnCdS@MoS2 heterostructured cages and then used it as PEC aptasensor for lincomycin detection. The result displayed that the PEC aptasensor exhibited a wide liner work range response with a low detection limit for lincomycin detection, which attributed to the synergy between tailored hierarchical hollow structure and close contact heterojunction interface.

Recently, as an important member of ternary chalcogenide, $ZnIn_2S_4$ with two-dimensional (2D) flower-like structures has triggered wide attention in photocatalysis thanks to its excellent optical and electrical performance, perfect chemical stability and extremely high specific surface area. What is more, $ZnIn_2S_4$ has an appropriate band gap, which not only endows it strong visible light harvesting ability, but also can make it match with g-C_3N_4. This is benefited to construct the binary $ZnIn_2S_4$/g-C_3N_4 heterojunction to enhance the photogenerated electron/hole separation and migration efficiency [25–27]. In recent reports, $ZnIn_2S_4$/g-C_3N_4 heterojunction has been synthesized and applied to photocatalytic H_2 production [26] and photodegradation pollution [27]. However, there were rarely reports that $ZnIn_2S_4$/g-C_3N_4 heterojunction was used as PEC sensor.

Herein, binary 2D/2D $ZnIn_2S_4$/g-C_3N_4 heterojunction was easily obtained *via* a simple hydrothermal method. The scanning electronic microscopy (SEM), transmission electron microscopy (TEM)

* Corresponding author.
E-mail address: zhaichunyang@nbu.edu.cn (C. Zhai).

https://doi.org/10.1016/j.cclet.2021.07.047
1001-8417/

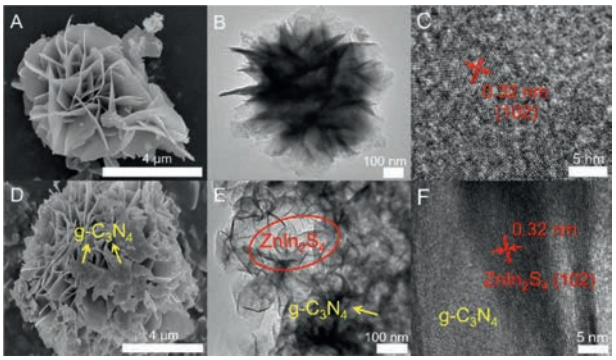

Fig. 1. SEM (A, D), TEM (B, E) and HRTEM (C, F) images of $ZnIn_2S_4$ (A-C) and $ZnIn_2S_4$/g-C_3N_4 (D-F).

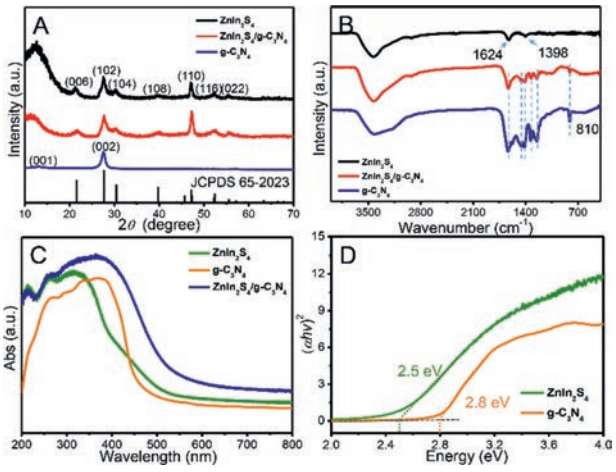

Fig. 2. XRD patterns (A), FT-IR spectra (B) and UV-vis diffuse reflection spectra (C) of samples. Plot (D) of $(\alpha h\nu)^2$ *vs. hv* for the band gap energy of $ZnIn_2S_4$ and g-C_3N_4.

and high-resolution transmission electron microscopy (HRTEM) were offered to survey the morphology of $ZnIn_2S_4$ and $ZnIn_2S_4$/g-C_3N_4. Fig. 1A displays that pure $ZnIn_2S_4$ exhibits globular flower-like structure with multiple nanosheets and the TEM image of $ZnIn_2S_4$ (Fig. 1B) is in good agreement with it. Fig. 1C shows the high-resolution (HR-TEM) image of $ZnIn_2S_4$, in which the lattice spacing (~0.32 nm) is ascribed to (102) crystal plane of $ZnIn_2S_4$. Fig. 1D shows that $ZnIn_2S_4$/g-C_3N_4 heterojunction inherits the flower-like structure of $ZnIn_2S_4$ and g-C_3N_4 nanosheets attach to the surface visually in addition. The TEM and HR-TEM (Figs. 1E and F) further testify that $ZnIn_2S_4$ and g-C_3N_4 have been in sufficient contacted and formed an effective heterogeneous junction interface.

The crystal structure of samples was investigated by X-ray powder diffraction (XRD) as revealed in Fig. 2A. One can see that the characteristic diffraction peaks in $ZnIn_2S_4$/g-C_3N_4 are great correspondence relations with the hexagonal $ZnIn_2S_4$ (JCPDS No. 65-2023), implying that crystalline structure of $ZnIn_2S_4$ is not be noticeably affected by the introduction of g-C_3N_4 [28,29]. However, the coincidence of (002) crystal plane of g-C_3N_4 and (102) crystal plane of $ZnIn_2S_4$ may render us uncertain whether g-C_3N_4 has been correctly introduced. To deeply verify the presence of g-C_3N_4 in $ZnIn_2S_4$/g-C_3N_4, Fourier transform infrared spectroscope (FT-IR) test was performed (Fig. 2B). For pure $ZnIn_2S_4$, two adsorption peaks appear at 1398 cm^{-1} and 1624 cm^{-1} are associated with the physical absorption of water molecules and hydroxyl groups [30]. For pure g-C_3N_4, several strong peaks found within the limit of 1200-1650 cm^{-1} are ascribed to the typical stretching modes of g-C_3N_4 heterocycles. The board band in 3000–3500 cm^{-1} region is attributed to the stretching modes of NH heterocycles and the strong characteristic vibration mode derives from the triazine units results in the sharp peak at 810 cm^{-1} [31,32]. Compare with pure g-C_3N_4, all main adsorption peaks emerge in the FT-IR spectra of $ZnIn_2S_4$/g-C_3N_4, which verify that the successful preparation of the heterojunction.

The optical properties of the samples were characterized by the UV-Vis diffuse reflectance spectra (DRS) (Fig. 2C). The absorption edge of pure g-C_3N_4 is around 460 nm and pure $ZnIn_2S_4$ shows about 550 nm. For $ZnIn_2S_4$/g-C_3N_4 heterojunction, the absorption edge extends to 580 nm, guessing that the interaction of $ZnIn_2S_4$ and g-C_3N_4 made an essential contribution to broaden the absorption in the visible range [33]. The bandgap energy (E_g) could be determined by the following equation: $\alpha h\nu = A(h\nu - E_g)^{n/2}$, in which α, $h\nu$, A represent the absorption coefficient, light frequency and a constant, respectively. The index n is decided by the type of semiconductor ($n = 1$ for direct transition and $n = 4$ for indirect transition) and $ZnIn_2S_4$ and g-C_3N_4 are both the direct-transition type in terms of previously reports [34]. Combine the above-mentioned with Fig. 2D, the E_g of $ZnIn_2S_4$ and g-C_3N_4 is denoted as 2.5 eV and 2.8 eV, which is close to the literature value [35,36]. Besides, the equations of $E_{VB} = \chi - E_e + 0.5\ E_g$ and $E_{CB} = E_{VB} - E_g$ are used to calculate the valence band (VB) and conduction band (CB) energy levels of semiconductors, where E_{VB} and E_{CB} are the energy of VB and CB, E_e (~ 4.5 eV) is the energy of free electrons on the hydrogen scale, χ is the geometric mean of the absolute electronegativity of the constituent atoms (4.86 eV for $ZnIn_2S_4$, 4.63 eV for g-C_3N_4) [37,38]. Accordingly, the E_{VB} of $ZnIn_2S_4$ and g-C_3N_4 is assigned to be + 1.61 eV and + 1.53 eV, and the E_{CB} of $ZnIn_2S_4$ and g-C_3N_4 was -0.89 eV and -1.27 eV, respectively.

The X-ray photoelectron spectroscopy (XPS) analysis was conducted to probe the elemental valence state and composition of samples in depth. Fig. S1A (Supporting information) checks all characteristic peaks entailed by C, N, Zn, In, S elements, indicating $ZnIn_2S_4$ and g-C_3N_4 have already presented in the heterojunction. As shown in Fig. S1B (Supporting information), three peaks of the C 1s spectrum, which center at 288.4 eV and 284.9 eV, are attributed to N–C=N bonds and C-C bonds, and 285.9 eV is interpreted as defect-containing sp^2-hybridized carbon in g-C_3N_4 surface [39]. For the N 1s spectrum (Fig. S1C in Supporting information), three peaks refer to C-N-H bonds (401.2 eV), N–C_3 bonds (400.1 eV) and C–N=C bonds (398.8 eV) [30,40]. By contrast, the peaks negatively shift to 0.2 and 0.4 eV in the C 1s and N 1s spectrum of the binary systems respectively. Nevertheless, the Zn 2p, In 3d and S 2p spectrum underwent an opposite shift between $ZnIn_2S_4$ and $ZnIn_2S_4$/g-C_3N_4. Figs. S1D-F (Supporting information) depicts that Zn $2p_{1/2}$ (1021.5 eV) and Zn $2p_{3/2}$ (1044.3 eV), In $3d_{3/2}$ (452.3 eV) and In $3d_{5/2}$ (444.5 eV), S $2p_{3/2}$ (162.78 eV) and S $2p_{1/2}$ (161.88 eV) in g-C_3N_4 increase to Zn $2p_{1/2}$ (1022.5 eV) and Zn $2p_{3/2}$ (1045.6 eV), In $3d_{3/2}$ (452.5 eV) and In $3d_{5/2}$ (444.88 eV), S $2p_{3/2}$ (162.96 eV) and S $2p_{1/2}$ (161.92 eV) in $ZnIn_2S_4$/g-C_3N_4, respectively [41]. Theoretically, the changes of binding energy are related to the gain and loss of electrons, which not only prove the successfully synthesis of target heterojunction, but also substantiate the existence of active surface electron transfer between the two materials [42,43].

Electrochemical impedance spectroscopy (EIS) is the best appropriate method to study the electron transfer of different materials. In Nyquist diagram, the smaller the semicircle diameter, the smaller the impedance, implying the faster the electron transfer rate [44]. Distinctly, the electron-transfer resistances (R_{ct}) of the samples in owning of visible light are smallest (Fig. S2A in Supporting information), which is probably interpreted that the heterojunction interface can act as a connecting bridge to accelerate electron transfer rate, which accelerates the separation rate of photogenic electron/hole pairs with the assistance of

visible light [45,46]. Additionally, differential pulse voltammetry (DPV) determination was carried out in phosphate buffered solution (PBS) containing 50 mmol/L BPA to demonstrate the photoelectrocatalytic performance of the $ZnIn_2S_4$/g-C_3N_4 modified electrode. Fig. S2B (Supporting information) displays that there has little difference in current density for pure $ZnIn_2S_4$, however, there exists a relatively large otherness of current density to $ZnIn_2S_4$/g-C_3N_4 heterojunction with or without visible light. As shown in Fig. S2C, the peak current density of $ZnIn_2S_4$/g-C_3N_4 (36.57 mA/cm^2) with visible-light irradiation is 1.88 times more than that without visible-light. Moreover, the oxidation peak potential slightly shifts negatively, speculating that the formation of heterojunction works positively.

For further understanding the electrocatalytic mechanism of BPA on $ZnIn_2S_4$/g-C_3N_4 modified electrode, Cyclic Voltammetry (CV) was employed at different scan rates (40–240 mV/s). Figs. S3A-C (Supporting information) displays that the oxidation peak shifts gradually towards positive potential and the peak current (I_p) increases linearly with the scan rate (v) ($R^2 = 0.99914$), which demonstrates that the process is controlled by absorption [47]. According to the Laviron's equation ($E_p = E^\theta + (\frac{RT}{\alpha nF})\ln(\frac{RTk^\theta}{\alpha nF}) + \frac{RT}{\alpha nF}\ln v$) where $E^\theta, k^\theta, \alpha, n, v, R, T$ and F mean formal redox potential, (standard rate constant of the reaction, transfer coefficient, electron transfer number, scan rate, gas constant, absolute temperature and Faraday's constant, respectively), it can be calculated that n $\approx$ 2 (taking α = 0.5, T = 298 K, R = 8.314 J K^{-1} mol^{-1}, and F = 96480 C/mol). Thus, it can be speculated that the electrocatalytic oxidation of BPA might be a two-electron and two-proton process [48–50].

The influence of PBS pH value was investigated in the range of 5.0-10.0. As illustrated in Figs. S3D-F (Supporting information), the current density shows a trend of increasing first and then decreasing, reaching the maximum value at 8.0. The pH of maximal current response is lower than the pK_a of BPA (pK_a = 9.73), indicating the undissociated BPA molecules could be adsorbed better than the dissociated ionic BPA on the $ZnIn_2S_4$/g-C_3N_4 modified electrode surface [9]. So that, the optimal pH value of 8.0 is chosen in the subsequent experiments. In addition, the linear relation of the oxidation potential (E_p) and pH is expressed as: E_p = – 0.06194pH + 0.97524 (R^2 = 0.99327) in Fig. S3F and by which, the obtained slope approximate to the theoretical value (57.6 mV per pH) [9,51]. It indicates that the electron transfer was accompanied by an equal number of protons in electrode reaction, further certifying that the oxidation process would be a two-electron and two-proton process. As can be seen from Fig. S4A (Supporting information), the longer the deposition time, the greater the measured current, and the oxidation peak current density levels off after 240 s, meaning that the adsorbance tends to saturation at 240 s. Furthermore, in order to investigate the effect of current response of the coating amount of $ZnIn_2S_4$/g-C_3N_4 on electrode, different amount of the samples are coated on the electrode surface. It is clearly shown that 5 mL is the optimum (Fig. S4B in Supporting information), which supposes that the appropriate accumulation of coating volume is responsible to improve the abilities of conductivity and adsorption, while excessive thickness of the electrode surface may impede the electron transfer rate, thus resulting in the dropping of current density.

DPV determination was also seized to evaluate the analytical performance of $ZnIn_2S_4$/g-C_3N_4 modified electrode under the optimal conditions (pH 8.0 of PBS, 240 s of deposition time, 5 mL of coating amount) and the concentration of BPA from 0.05 mmol/L to 30 mmol/L. Fig. 3A displays that the oxidation peak current density is enhanced continuously with increasing the BPA concentration. Moreover, the oxidation potential shifts negatively with the advancing of concentration, indicating that the oxidation enhanced

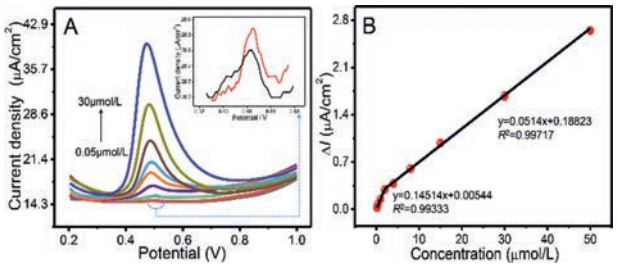

Fig. 3. DPV (A) of $ZnIn_2S_4$/g-C_3N_4 modified electrode in PBS (pH 8.0) possessing different concentration of BPA (0.05, 0.06, 0.1, 0.4, 1, 2, 4, 8, 15, 30 mmol/L) with visible-light irradiation, insert: DPV of 0.05 and 0.06 mmol/L BPA concentration. The linear relationship (B) of various concentrations *vs.* current response.

accordingly. As depicted in Fig. 3B, the two regression curves could be received: $I = 0.14514c + 0.00544$ ($R^2 = 0.99333$) in the range of 0.05 mmol/L to 2 mmol/L; $I = 0.0514\ c + 0.18823$ ($R^2 = 0.99717$) in the range of 2 mmol/L to 30 mmol/L. On account of the signal-to-noise ratio is equal to 3 (S/N = 3), the detection limit was estimated to be 0.016 mmol/L. As depicted in Table S1 (Supporting information), which demonstrates the desired results such as detection limits obtained by the proposed sensing system are superior or comparable with others. It also denotes that the $ZnIn_2S_4$/g-C_3N_4 heterojunction has a bright application prospect in PEC detecting BPA.

The reproducibility and stability of the $ZnIn_2S_4$/g-C_3N_4 modified electrode (Figs. S5A and B in Supporting information) are investigated by DPV determination in PBS with 5 mmol/L BPA. Firstly, six individual electrodes are utilized to measure the reproducibility and the relative standard deviation (RSD) is 3.07%. Then, stability is estimated every two days. After two weeks, the result displays that the current responses of seven times stay over 90% and the RSD is 4.60%. Based on the above tests, the $ZnIn_2S_4$/g-C_3N_4 modified electrode has well reproducibility and stability. It is indispensable to study the interference test due to the complexity of the real environment. Some possible interfering substances including inorganic ions (Cl^-, Na^+, Cu^{2+}, SO_4^{2-}) and organic compounds (glucose, *p*-acetamidophenol, catechol) were selected to examine in 5 mmol/L BPA-contained PBS. The validation results as described in Fig. S5C (Supporting information) reveals that both inorganic ions and organic compounds have slight influence on the BPA detection. For chasing the applicability and sensitivity of as-synthesized material in real sample, the $ZnIn_2S_4$/g-C_3N_4 modified electrode was used to detect BPA in the real water samples. Table S2 (Supporting information) shows that the average recovery rates of BPA in real water samples including river water, tap water and seawater are in the scope of 92.6% to 104.7%, signifying that as a novel PEC sensor, the $ZnIn_2S_4$/g-C_3N_4 modified electrode is feasible for the detection of BPA in real samples.

The possible mechanism to use $ZnIn_2S_4$/g-C_3N_4 modified electrode for photoelectrochemical detection of BPA is proposed and presented in Scheme 1. Thanks to the special flower-like structures of $ZnIn_2S_4$, large amounts of BPA are adsorbed on the surface of $ZnIn_2S_4$/g-C_3N_4 heterojunction. As a typical electrochemical (EC) sensor of $ZnIn_2S_4$/g-C_3N_4, BPA is easily oxidized and loses two electrons through the DPV method, resulting in a corresponding current response. Under the visible-light irradiation, $ZnIn_2S_4$/g-C_3N_4 is excited to generate electrons and holes in the conduction band and valence band, respectively. Due to the E_{CB} of g-C_3N_4 being more negative than that of $ZnIn_2S_4$, the light-generated electrons could move from the conduction band of g-C_3N_4 to $ZnIn_2S_4$ on the action of $ZnIn_2S_4$/g-C_3N_4 heterojunction. At the same time, because of the smaller E_{VB} of g-C_3N_4, the photo-generated holes can transfer from the valence band of $ZnIn_2S_4$ to g-C_3N_4. The

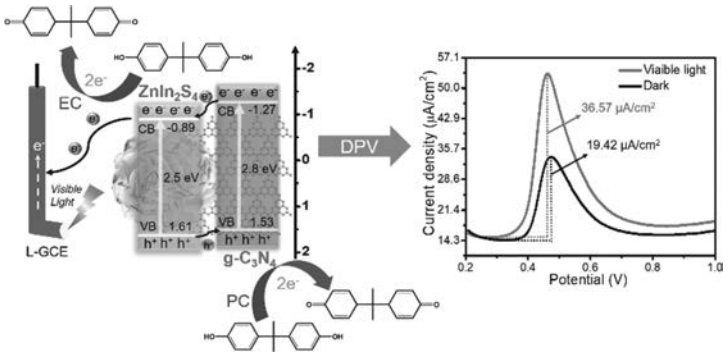

Scheme 1. The mechanism of photoelectrochemical detection for BPA on the $ZnIn_2S_4$/g-C_3N_4 modified electrode.

above process can help to promote the separation efficiency of light-generated electrons/hole pairs. More importantly, the photo-generated holes with strong oxidation ability can directly oxidize H_2O/OH^- to ·OH. Both ·OH and photo-generated holes can oxidize the BPA adsorbing on the surface of $ZnIn_2S_4$/g-C_3N_4 heterojunction, which further enhances the corresponding current response signal during electrochemical detection.

In summary, a binary PEC sensor has been prepared to detect BPA on the basis of $ZnIn_2S_4$/g-C_3N_4 heterojunction. The PEC conversion efficiency improved remarkably because of the matched band structures of $ZnIn_2S_4$ and g-C_3N_4 and the photoelectric synergistic effect, leading to an obviously amplified photocurrent response signal of BPA detection when $ZnIn_2S_4$/g-C_3N_4 modified electrode was used as a sensor. In other words, the PEC sensor displayed an appreciable detection sensitivity, remarkable stability and reproducibility, low detection limit, and wide liner range for the determination of BPA. These results provide a novel facile strategy for the establishment of sensitive BPA photoelectrochemical sensors.

Declaration of competing interest

The authors declare that they have no known competing financial interests or personal relationships that could have appeared to influence the work reported in this paper.

Acknowledgment

The present study was supported by the Key Laboratory of Resource Chemistry, Ministry of Education (No. KLRC_ME2002).

Supplementary materials

Supplementary material associated with this article can be found, in the online version, at doi:10.1016/j.cclet.2021.07.047.

References

[1] L.J. Ling, J.P. Xu, Y.H. Deng, et al., Anal. Methods 10 (2018) 2722–2730.
[2] P. Jing, X.M. Zhang, Z.X. Wu, et al., Talanta 141 (2015) 41–46.
[3] S.J. Hu, Y.J. Yu, Y. Guan, et al., Chin. Chem. Lett. 31 (2020) 2839–2842.
[4] L. Shi, Y. Yin, L.C. Zhang, et al., Appl. Catal. B: Environ. (2019) 405–422.
[5] J. Shu, D.P. Tang, Anal. Chem. 92 (2020) 363–377.
[6] L.W. Yang, S. Zhang, X.Q. Liu, et al., J. Mater. Chem. B 8 (2020) 7880–7893.
[7] A. Thamilselvan, V. Rajagopal, V. Suryanarayanan, J. Alloy. Compd. 786 (2019) 698–706.
[8] P.C. Yan, Z. Mo, L. Xu, et al., Electrochim. Acta 319 (2019) 10–17.
[9] B.Y. Su, H.L. Shao, N. Li, et al., Talanta 166 (2017) 126–132.
[10] N.B. Messaoud, M.E. Ghica, C. Dridi, M.B. Ali, C.M.A. Brett, Sensor. Actuat. B: Chem. 253 (2017) 513–522.
[11] D.N. Pei, A.Y. Zhang, X.Q. Pan, Y. Si, H.Q. Yu, Anal. Chem. 90 (2018) 3165–3173.
[12] X.Y. Bai, Y. Zhang, W.K. Gao, et al., Biosens. Bioelectron. 168 (2020) 112522.
[13] X. Zhang, J.J. Peng, Y.P. Ding, et al., Sensor. Actuat. B: Chem. 306 (2020) 127552.
[14] Y.S. Chang, P.Y. Hsieh, T.F.M. Chang, et al., J. Mater. Chem. A 8 (2020) 13971–13979.
[15] L.N. Wang, X.Q. Shi, Y.F. Jia, et al., Chin. Chem. Lett. 32 (2021) 1869–1878.
[16] Y.F. Li, M. Zhang, L. Zhou, et al., Acta. Phys-Chim. Sin. 37 (2021) 2009030.
[17] S.J. Sun, H. Ding, L.F. Mei, et al., Chin. Chem. Lett. 31 (2020) 2287–2294.
[18] M. Ismael, J. Alloy. Compd. 846 (2020) 156446.
[19] Z.D. Wei, J.Y. Liu, W. Shangguan, Chin. J. Catal. 41 (2020) 1440–1450.
[20] Z.R. Zhou, Y.N. Li, M.M. Li, Y. Li, S.H. Zhan, Chin. Chem. Lett. 31 (2020) 2698–2740.
[21] M.C. Yu, H.J. Liang, R.N. Zhan, L. Xu, J.F. Niu, Chin. Chem. Lett. 32 (2021) 2155–2158.
[22] L.Y. Meng, Y. Qu, L.Q. Jing, Chin. Chem. Lett. 32 (2021) 3265–3276.
[23] S.Y. Yu, L. Zhang, L.B. Zhu, et al., Coordin. Chem. Rev. 393 (2019) 9–20.
[24] Z.G. Wu, J.L. Zhao, Z.K. Yin, et al., Sensor. Actuat. B: Chem. 312 (2020) 127978.
[25] W. Chen, T.Y. Liu, T. Huang, X.H. Liu, X.J. Yang, Nanoscale 8 (2016) 3711–3719.
[26] B. Lin, H. Li, H. An, et al., Appl. Catal. B: Environ. 220 (2018) 542–552.
[27] H.C. Yang, R.Y. Cao, P.X. Sun, et al., Appl. Catal. B: Environ. 256 (2019) 117862.
[28] T.M. Su, Z.D. Hood, M. Naguib, et al., Nanoscale 11 (2019) 8138–8149.
[29] Y.J. Chen, S.W. Hu, W.J. Liu, et al., Dalton. T 40 (2011) 2607–2613.
[30] Z. Zhang, K. Liu, Z. Feng, Y. Bao, B. Dong, Sci. Rep. 6 (2016) 19221.
[31] S.C. Yan, Z.S. Li, Z.G. Zou, Langmuir 25 (2009) 10397–10401.
[32] L.S. Jiang, Y. Xie, F. He, et al., Chin. Chem. Lett. 32 (2021) 2187–2191.
[33] B. Zhang, H. Wang, J. Xi, F. Zhao, B. Zeng, Sensor. Actuat. B: Chem. 298 (2019) 126835.
[34] H. Liu, Z.T. Jin, Z.Z. Xu, Z. Zhang, D. Ao, RSC. Adv. 5 (2015) 97951–97961.
[35] S.B. Wang, B.Y. Guan, X.W.D. Lou, J. Am. Chem. Soc. 140 (2018) 5037–5040.
[36] J.W. Fu, J.G. Yu, C.J. Jiang, B. Cheng, Adv. Energy Mater. 8 (2018) 1701503.
[37] Q. Zhu, Y. Sun, S. Xu, et al., J. Hazard. Mater. 382 (2020) 121098.
[38] W.K. Jo, T.S. Natarajan, J. Colloid. Interf. Sci. 482 (2016) 58–72.
[39] Y.X. Wang, F.T. He, L. Chen, et al., Chin. Chem. Lett. 31 (2020) 2668–2672.
[40] C.S. Lei, W. Zhou, L.J. Shen, et al., ACS Sustain. Chem. Eng. 7 (2019) 16257–16263.
[41] D.X. Yang, J.L. Liang, L. Luo, et al., Chin. Chem. Lett. 32 (2021) 2534–2538.
[42] S. Tonda, S. Kumar, M. Bhardwaj, P. Yadav, S. Ogale, ACS Appl. Mater. Inter. 10 (2018) 2667–2678.
[43] Y.Y. Qin, H. Li, J. Lu, et al., Appl. Catal. B: Environ. 277 (2020) 119254.
[44] P.C. Yan, L. Xu, D.S. Jiang, et al., Electrochim. Acta 259 (2018) 873–881.
[45] Z. Li, H.M. Zhang, Q.B. Zha, et al., Microchim. Acta 187 (2020) 526.
[46] D.L. Yuan, M.T. Sun, S.F. Tang, et al., Chin. Chem. Lett. 31 (2020) 547–550.
[47] Y.H. Pang, Y.Y. Huang, L. Wang, X.F. Shen, Y.Y. Wang, Environ. Pollut. 263 (2020) 114616.
[48] Y.Z. Zhou, L.Y. Yang, S.L. Li, Y. Dang, Sensor. Actuat. B: Chem. 245 (2017) 238–246.
[49] D.N. Pei, A.Y. Zhang, X.Q. Pan, Y. Si, H.Q. Yu, Anal. Chem. 90 (2018) 3165–3173.
[50] Y.H. Pang, L. Wang. Y.Y. Huang, X.F. Shen, Y.Y. Wang, Environ. Pollut. 263 (2020) 114616.
[51] Y.Z. Zhou, L.H. Yang, S.H. Li, Y. Dang, Sensor. Actuat. B: Chem. 245 (2017) 238–246.